Published in final edited form as:
*J Comput Neurosci*. 2010 August ; 29(1-2): 49–62. doi:10.1007/s10827-010-0228-5.

# Methods for predicting cortical UP and DOWN states from the phase of deep layer local field potentials

**Aman B. Saleem**,
Department of Bioengineering, Imperial College London, London SW7 2AZ, UK

**Paul Chadderton**,
UCL Ear Institute, 332 Grays Inn Road, London WC1X 8EE, UK

Center for Molecular and Behavioral Neuroscience, Rutgers University, 197 University Avenue, Newark, NJ 07102, USA

**John Apergis-Schoute**,
Department of Bioengineering, Imperial College London, London SW7 2AZ, UK

**Kenneth D. Harris**, and
Department of Bioengineering, Imperial College London, London SW7 2AZ, UK

Center for Molecular and Behavioral Neuroscience, Rutgers University, 197 University Avenue, Newark, NJ 07102, USA

**Simon R. Schultz**
Department of Bioengineering, Imperial College London, London SW7 2AZ, UK

## Abstract

During anesthesia, slow-wave sleep and quiet wakefulness, neuronal membrane potentials collectively switch between de- and hyperpolarized levels, the cortical UP and DOWN states. Previous studies have shown that these cortical UP/DOWN states affect the excitability of individual neurons in response to sensory stimuli, indicating that a significant amount of the trial-to-trial variability in neuronal responses can be attributed to ongoing fluctuations in network activity. However, as intracellular recordings are frequently not available, it is important to be able to estimate their occurrence purely from extracellular data. Here, we combine *in vivo* whole cell recordings from single neurons with multi-site extracellular microelectrode recordings, to quantify the performance of various approaches to predicting UP/DOWN states from the deep-layer local field potential (LFP). We find that UP/ DOWN states in deep cortical layers of rat primary auditory cortex (A1) are predictable from the phase of LFP at low frequencies (< 4 Hz), and that the likelihood of a given state varies sinusoidally with the phase of LFP at these frequencies. We introduce a novel method of detecting cortical state by combining information concerning the phase of the LFP and ongoing multi-unit activity.

### Keywords

UP and DOWN states; LFP; State dependent coding; Neural coding; Spontaneous activity; Neural oscillations



aman.saleem04@imperial.ac.uk.

**Action Editor: Daniel Krzysztof Wojcik**

**Electronic supplementary material** The online version of this article (doi:10.1007/s10827-010-0228-5) contains supplementary material, which is available to authorized users.

## 1 Introduction

During the variety of behavioral conditions encountered through the day, the cortex switches between different internal conditions, each characterized by distinctive spatiotemporal patterns of activity. Brain states relating to vigilant or active behavior involve small amplitude but high frequency fluctuations in electroencephalogram (EEG) recordings, local field potential (LFP) and neuronal membrane potential ($V_m$)—the "desynchronized" state (Steriade et al. 2001; Timofeev et al. 2001; Crochet & Peterson 2006; Poulet & Petersen 2008). In comparison, slow-wave sleep, some types of anesthesia, and quiet wakefulness result in slow (< 1 Hz) large-amplitude oscillations in EEG and LFP, the "synchronized" state, during which there are related shifts in membrane potential between depolarized 'UP' and hyperpolarized 'DOWN' states (Steriade et al. 1993; Cowan & Wilson 1994; Lampl et al. 1999; Sanchez-Vives & McCormick 2000; reviewed in Destexhe et al. 2007). The functional implications of these UP/DOWN states have been of much recent interest to both experimental and computational neuroscientists (Haider et al. 2007; Li et al. 2009; Compte et al. 2003; Holcman & Tsodyks 2006; Parga & Abbott 2007; Hoffman et al. 2007; Destexhe 2009; Luczak et al. 2009) however little is yet known about how they support information processing in brain circuitry.

Commonly used anesthetics that induce the "synchronized" state have allowed researchers to investigate the dependence of cortical network dynamics during UP and DOWN states, in a relatively controlled and stable manner. Examining different cortical processes ranging from synaptic plasticity (Crochet and Peterson 2006; Reig et al. 2006), network dynamics (Cossart et al. 2003; Haider et al. 2006; Sanchez-Vives and McCormick 2000; Shu et al. 2003; Luczak et al. 2007; Sakata and Harris 2009), and sensory integration (Hasenstaub et al. 2007; Lampl et al. 1999; Petersen et al. 2003; Sachdev et al. 2004) during UP and DOWN states has allowed researchers to probe how internal brain UP/DOWN state dynamics affects basic cortical computations. A number of studies have shown that sensory-evoked synaptic responses are strongly dependent on the instantaneous UP/DOWN state of the cortex (Anderson et al. 2000; Arieli et al. 1996; Azouz and Gray 1999; Haider et al. 2007; Petersen et al. 2003; Sachdev et al. 2004; Curto et al. 2009) suggesting that much of the trial-to-trial variability in sensory-driven responses might be explained by spontaneous fluctuations in cortical UP/DOWN states.

Most of these studies relied on challenging *in vivo* intracellular recordings to accurately gauge the UP/DOWN state of the network by measuring changes in membrane potential. High-density extracellular electrodes have now made it possible to begin looking at the state-dependence of population coding by relating the activity of tens of neurons recorded simultaneously to measured external variables. Consequently, an alternative method (to intracellular recordings) for accurately characterizing the instantaneous state of cortical neural networks would be likely to prove extremely useful in probing the state dependence of cortical information coding and processing.

During transitions of the membrane potential between UP and DOWN states the LFP shows characteristics such as a depth positive deflection during a transition to an UP state (Creutzfeldt et al. 1966a, b; Contreras and Steriade 1995, reviewed in Destexhe et al. 2007). However, it is unclear as to which features of the LFP waveform best reflect cortical UP and DOWN states, and whether these features are exclusive to the state transitions. To determine the relationship between LFP phase and membrane potential we recorded *in vivo* intracellular activity of neurons in the cortex while simultaneously monitoring the LFP and the activity of multiple cells in the region using a multi-electrode array. The recordings reveal that during cortical UP/DOWN states there is a strong relationship between the phase

of low frequency LFP (< 4 Hz) of the deep cortical layers, and the membrane potential of the neuron. Based on this relationship, we have developed a method for determining cortical UP and DOWN states from LFP alone, or in combination with multi-unit activity. We quantitatively compare the performance of various methods of detecting cortical UP and DOWN states during synchronized network activity. Our results provide a novel method for detecting cortical state by combining information regarding the phase of the LFP and ongoing multi-unit activity which correctly allocates time bins to cortical UP/DOWN states with over 90% accuracy.

## 2 Methods

### 2.1 Experimental procedures

All procedures for animal care and experimentation were approved by the Institutional Animal Care and Use Committee of Rutgers University. Sprague-Dawley rats (P21–28) were anesthetized with urethane (1.5 g/kg) via intraperitoneal injection (i.p.). Body temperature was maintained at 37°C using a feedback-controlled heating pad (FHC, Bowdoin, ME, USA). When animals were areflexive, they were secured in a customized naso-orbital restraint. A craniotomy was performed over primary auditory cortex (A1; 3.5 mm posterior, 7 mm lateral of bregma; Paxinos and Watson 2004), and the dura was removed under a high-magnification dissecting microscope. Silicon microelectrodes (NeuroNexus Technologies, Ann Arbor, MI, USA) were inserted into A1 via a manual manipulator (Model 1460, Kopf Instruments, Tujunga, CA, USA). Probes had four shanks spaced by 200 μm, with eight recording sites per shank, as schematically illustrated in Fig. 1(a). On each shank, recording sites were arranged in a dual tetrode configuration, each separated by 150 μm (25 μm intra-tetrode spacing between sites). The bottom layer of tetrodes was positioned in deep layers of the cortex, most likely layer V, as determined by field potential reversal (Kandel and Buzsaki 1997).

Following positioning of the silicon probe, low resistance patch pipettes (4–6 MΩ) were lowered onto the surface of the brain, as close to the silicon probe as possible using an automated micromanipulator (SM-4; Luigs and Neumann, Ratingen, Germany). A Multiclamp 700B amplifier (Molecular Devices, Sunnyvale, CA, USA) was then used to search for, and record from neurons *in vivo*. The internal solution contained (in mM): K-Gluconate 130, Na-Phosphocreatine 10, HEPES 10, KCl 7, Mg-ATP 4, $Na_2$-GTP 0.5, EGTA 0.05. Blind whole cell recordings of membrane potential were made from individual A1 pyramidal cells during simultaneous recording of extracellular multi-unit (MUA) and local field potential (LFP) activity via the silicon microelectrode (a ‘patch-probe’ configuration). Figure 1 illustrates this recording configuration, and also shows typical membrane potential, LFP and MUA recordings.

During recording, patch-probe activity was monitored during silence (‘spontaneous’), and during auditory stimulation via ongoing 1 Hz sinusoidal amplitude-modulated white noise (‘AM noise’), and pure tone presentation (‘tone’). Auditory stimulation was delivered through a calibrated electrostatic loudspeaker (ES-1, Tucker-Davis Technologies, Alachua, FL, USA) in a single-walled soundproof box (IAC, USA) covered by 7.5 cm of acoustic absorption foam. Pure tones of 50 or 100 ms duration were presented in a randomized order at 2 Hz (1/6 octave steps, 3–48 kHz; 10 dB steps, 0–80 dB SPL). Sinusoidal amplitude-modulated noise had a mean intensity of 60 dB SPL.

Broadband signals (> 1 Hz) from the silicon probe were amplified (×1,000) using a 32-channel amplifier (Plexon, Dallas, TX, USA). Whole cell patch clamp data were low-pass filtered at 3 kHz. All data were digitized at 20 kHz and stored on a hard drive. Offline,

spiking sorting procedures were performed as previously described (Bartho et al. 2004, Luczak et al. 2007) and data were analyzed using Matlab (Mathworks, Natick, MA, USA).

The findings presented in this manuscript regarding the relationship between the LFP/MUA and the cortical UP/ DOWN states are consistent across all the recordings, during spontaneous and stimulus–evoked epochs. All data are presented as mean±s.e.m for $n$=9 recordings unless otherwise stated.

### 2.2 Detecting cortical UP/DOWN state from membrane potential

Neuronal membrane potentials switch from a depolarised level during an UP state to a hyperpolarised level during a DOWN state. This shift in the membrane potential has previously been used to detect cortical UP/DOWN states (Wilson and Groves 1981; Wilson and Kawaguchi 1996; Anderson et al 2000; Hasenstaub et al 2007; Poulet and Petersen 2008). Membrane potential traces were median filtered to remove spikes and then smoothed by low-pass filtering at 20 Hz (see Fig. 2(a, b)). The distribution of the filtered membrane potential (Fig. 2(c)) shows the bimodal characteristics expected from a bistable system. However, there is a region of overlap making state distinction non-trivial. An expectation maximization algorithm was used to fit this distribution by a mixture of two Gaussians with means $\mu_{UP}$ & $\mu_{DOWN}$, and standard deviations $\sigma_{UP}$ & $\sigma_{DOWN}$. Periods of time in which filtered membrane potential was above ($\mu_{UP}$-$\sigma_{UP}$) were considered to be cortical UP states, and below ($\mu_{DOWN}$ + $\sigma_{DOWN}$) as cortical DOWN states. Figure 2(b and c) show the detection thresholds applied to the filtered membrane potential. We considered a switch in cortical state to occur only when the filtered membrane potential persisted above/below threshold for longer than 100 milliseconds. *P(UP)* is the overall probability of an UP state, and is calculated as:

$$P(UP)=\frac{\text{time in UP state}}{\text{total time}}. \quad (1)$$

P(DOWN) is similarly calculated. $P(UP)$ = 0:33 ± 0:03 and $P(DOWN)$ = 0:60 ± 0:02 under our anesthetic conditions (mean±s.e.m.). Note that $P(UP)$ and $P(DOWN)$ do not sum to 1 as there are some points in time that have an indeterminate state.

### 2.3 Analysis of multi-unit activity

We also sought to establish how accurately multi-unit activity could be used to detect cortical state. During our experiments, extracellular spiking was recorded from multiple sites simultaneously. As this allows different ways of acquiring and defining MUA, we calculated MUA using 3 different measures. The first measure, which we name “MUA:sin”, is similar to that used by Hasenstaub et al. (2007), with the exception that in their case MUA was recorded from a pipette rather than a single multi-electrode array recording site as used here. The recordings were rectified, median filtered (20 msec time window) and low pass filtered (at 25 Hz) to calculate MUA:sin. Note that in this case, no spike sorting was performed. As a second measure, we combined the spiking activity recorded from “spike sorted” single neuron activity across the four channels of a single tetrode, calling it “MUA:tet”. The combined activity was smoothed with a 100 millisecond Gaussian window to calculate “MUA:tet”. In the final measure, “MUA:all”, the spiking activity of neurons recorded on all the tetrodes in the recording (eight tetrodes; 32 recording sites) was used to calculate the MUA using a procedure similar to that for calculating MUA:tet. All the three MUA measures were normalized, by subtracting the minimum rate and dividing by the maximum rate, giving a resultant in the range of 0 to 1.

## 2.4 Analysis of LFP

The LFP recorded was low-pass filtered by 500 Hz and then downsampled from 20 kHz to 1 kHz. The down-sampled LFP was then filtered into different frequency bands (indexed by $X$, the ranges of $X$ are mentioned in the text and figures) using second order elliptic low or band pass filters (peak-to-peak ripple of 0.1 db and minimum stop-band attenuation of 40 db). To avoid phase delays from the filtering process we used zero-phase filters.

The phase $\phi_X(t)$ and power $k_X(t)$ at any time instant $t$ in the signal were calculated as the angle and amplitude of the Hilbert transform of the signal in each of the frequency bands $X$.

**2.4.1 Phase of LFP and cortical state—**Given the phase of the LFP, $\phi_X(t)$, in a particular frequency band $X$, we estimated the conditional probability of observing an UP state (based on $V_m$–detection of the state), $P(UP|\phi_X(t))$, as

$$P(UP|\phi_X(t)) = \frac{\#(UP|\phi_X(t))}{\#(\phi_X(t))}, \tag{2}$$

where #(x) represents the occurrence count of $x$. $P(DOWN|\phi_X(t))$ was estimated similarly.

We calculated the differential likelihood of states, $L_X(t)$, as

$$L_X(\phi_X) = P(UP|\phi_X(t)) - P(DOWN|\phi_X(t)), \tag{3}$$

in different frequency bands, where $X$ indexes the band. $L_X(\phi_X)$ ranges between −1 and 1. The relationships between $\phi_X(t)$ and $L_X$ are fitted to a sine wave by finding the $\theta_X(i)$ that yields the minimum value of:

$$MSE = \left( \sum_{\phi_X} \{L_X(\phi_X) - \cos[\phi_X - \theta_X(i)]\}^2 \right)^{1/2}, \tag{4}$$

where $i$ is the index of the recording. This is calculated for each of the $n$=9 recordings.

## 2.5 Detecting cortical UP/DOWN states from extracellular recordings

**2.5.1 Local field potential (LFP)—**The differential likelihood, $L_X$, measures the chance of an UP ($L_X$ close to 1) or DOWN ($L_X$ close to −1) state being observed. $L_X$ at any instant in time $t$ was approximated by $\tilde{L}_X(t)$ as:

$$\tilde{L}_X(t) = \cos(\phi_X(t) - \theta'_X(j)), \tag{5}$$

where $j$ is the index of the recording, $\phi_X(t)$ is the phase in the frequency band $X$ at time $t$. $\theta'_X(j)$ was calculated as mean of the $\theta_X(i)$'s of all other recordings, or:

$$\theta'_X(j) = \langle \theta_X(i) \rangle_{i \neq j}, \tag{6}$$

where $\langle\rangle$ indicates for the mean.

To detect cortical UP/DOWN states from LFP, the differential likelihood from different bands is combined to generate an evidence variable, $S_{LFP}$. $S_{LFP}(t)$ was used to detect the instantaneous state and was calculated as:

$$S_{LFP}(t)=\frac{1}{2}\left(1+\sum_{X}K_X(t)\tilde{L}_X(t)\right), \tag{7}$$

where $K_X(t)$ is the relative power of frequency band $X$ at time $t$, calculated as:

$$K_X(t)=\frac{k_X(t)}{k_{high}(t)+\sum_{X}k_X(t)}. \tag{8}$$

$k_{high}(t)$ is the power in the bands 20–40 Hz and 60– 100 Hz (we did not use the 40–60 Hz band to avoid mains noise). $K_X(t)$, or the 'L/(H+L) ratio', is a modification of the 'L/H ratio' (Li et al. 2009). This modification was made to limit $S_{LFP}$ between 0 and 1. As described in Li et al. (2009), the ratio of power between the low and high frequency bands, the L/H ratio, is high when the cortex is in a synchronized state and hence switching between UP and DOWN states. To the contrary, when the cortex has a high power in the higher frequency bands, it remains in a desynchronized state of activity and does not switch between UP and DOWN states. Consequently, the 'L/(H+L)' ratio remains low and reduces the evidence of UP and DOWN network states. By using the 'L/(H+L) ratio', random fluctuations in the lower frequencies of the LFP during desynchronized states, are not detected as switches in cortical UP/DOWN states (illustrated by Suppl. Fig. S1).

To determine the thresholds for detecting the instantaneous network state, the distribution of $S_{LFP}$ was first fitted by a mixture of three Gaussians using an expectation maximization algorithm. The means and variances of the Gaussians are represented as $\mu_{UP\text{-}LFP}$, $\mu_{IND\text{-}LFP}$& $\mu_{DOWN\text{-}LFP}$ and $\sigma_{UP\text{-}LFP}$, $\sigma_{IND\text{-}LFP}$ & $\sigma_{DOWN\text{-}LFP}$ for the UP, indeterminate and DOWN cortical states, respectively. The threshold for the detection of the UP states, was set as $\mu_{UP\text{-}LFP}-\sigma_{UP\text{-}LFP}$; and ($\mu_{DOWN\text{-}LFP}$ + $\sigma_{DOWN\text{-}LFP}$) for detecting DOWN states.

A receiver operating characteristic (ROC) analysis (Green and Swets 1966) was carried out by sliding the threshold, between the values of 0 and 1 (in steps of 0.05), along the decision variable $S_{LFP}$ (or $S_{MUA}$ and $S_{Comb}$ described later). We carried out the ROC analysis for UP state and DOWN state detection independently. For each threshold value chosen, the time instants defined as UP on the basis of $V_m$ which are also classified as UP states by the algorithm are considered to be 'true positives', while $V_m$-DOWN time instants classified as UP are considered to be 'false positives' for UP state detection.

**2.5.2 Multiunit activity (MUA)—**The multi-unit activity is used directly as the evidence variable to detect cortical state, or:

$$S_{MUA:yyy}=MUA:yyy, \tag{9}$$

where 'yyy' corresponds to either 'sin', 'tet' or 'all' as described in Section 2.4. Using an expectation maximization algorithm, the distribution of $S_{MUA:all}$ was first fitted by a mixture of two Gaussians, with means and variances, $\mu_{UP\text{-}MUA}$ & $\mu_{DOWN\text{-}MUA}$ and $\sigma_{\text{UP-MUA}}$ & $\sigma_{DOWN\text{-}MUA}$ for the cortical UP and DOWN state, respectively. The threshold for the

detection of UP states, was set as ($\mu_{UP\text{-}MUA} - \sigma_{UP\text{-}MUA}$); and ($\mu_{DOWN\text{-}MUA} + \sigma_{DOWN\text{-}MUA}$) for detecting DOWN states.

**2.5.3 Combination of LFP and MUA—**MUA and LFP both provide information about the cortical UP/DOWN states, and this may be to some extent independent information. This suggests that a strategy which combines evidence from both sources might be successful. If the information sources were in fact independent, the evidence could simply be linearly combined; this motivated use of the combined evidence variable, $S_{Comb}$:

$$S_{Comb} = \frac{1}{2}(S_{LFP} + S_{MUA:all}). \tag{10}$$

## 3 How do extracellular signals relate to network state?

How do the signals recorded with an extracellular electrode (LFP, MUA) relate to spontaneous network state changes? Can they in fact be used to infer the internal state of the surrounding tissue? We have explored this issue by using whole cell patch clamp recordings of membrane potential as a "ground truth" indicator of cortical (at least local) state, to examine the relationship between state transitions and the extracellular signal, LFP and MUA. Under the anesthesia conditions present in our study, UP states lasted for on average 221±15 ms, while DOWN states lasted for 360±18 ms (mean±s.e.m, across the 6 cells listed in Suppl. Table 1). The probability to be in a cortical UP state and DOWN state, under our anesthetic conditions, were $P(UP) = 0{:}33 \pm 0{:}03$ and $P(DOWN) = 0{:}60 \pm 0{:}02$ respectively (mean±s.e.m, across the 9 recordings listed in Suppl. Table 1). Note that $P(UP)$ and $P(DOWN)$ do not sum to 1 as there are some points in time that have an indeterminate state.

We extracted the times of DOWN to UP and UP to DOWN transitions from $V_m$, and used these to plot transition-triggered averages of MUA and LFP, shown in Fig. 2(d, e). The UP transition-triggered average MUA (Fig. 2(d)) shows that transitions to an UP state were accompanied by a significant increase in the multi-unit activity, peaking at 58.3±4.3 ms after $V_m$ -detected transitions. The increase in multi-unit activity lasted for a periods of ~200 ms, similar to the duration of states detected from $V_m$ (221±15 ms). Conversely, $V_m$-defined transitions to a DOWN state are followed by near silence of the multi-unit activity with a negative peak at 63.4±4 ms. These transition-triggered averages indicate that there is an increase in activity in the depolarized UP state and a decrease in the hyperpolarized DOWN state (see also Hasenstaub et al. 2007). It suggests that by sampling a large enough population of neurons, we should be able to determine the time at which a state transition occurs, an approach which has been used previously (Hasenstaub et al. 2007, Luczak et al. 2007, Renart et al. 2010). In fact, we found MUA to be strongly correlated with the membrane potential—MUA:sin had a Pearson correlation coefficient of 0.60±0.04 to $V_m$ (mean±s.e.m, across the 9 recordings listed in Suppl. Table 1), while MUA:tet gives a correlation of 0.61±0.04 and MUA:all a correlation of 0.69±0.03.

What features of the LFP waveforms relate most reliably to the occurrence of state transitions? Examination of Fig. 2(e) suggests that, if the LFP fluctuation occurring at around the time of a transition to an UP state were to be considered a "wave packet", then the state transition occurs at a particular phase within that wave packet—the phase that corresponds to the middle of the first, downwardly sloping deflection (see also Creutzfeldt et al. 1966a, b; Contreras and Steriade 1995) and the wave packets relating to DOWN transitions are centered about the point of symmetry, whereas those for UP transitions are substantially offset.

It is important to recall that the network is a dynamical system, and that its spontaneous dynamics reflect a continuous trajectory in a high dimensional space. We can observe this space in various ways, for instance by projecting it onto low dimensional variables (Luczak et al. 2009). One simple way to do this is to plot the joint trajectory of the recorded LFP and $V_m$ (Fig. 2(f)). This shows that it may in fact be possible to obtain a better estimate of cortical UP/DOWN state dynamics by using LFP and $V_m$ together rather than by using $V_m$ alone. Often we do not have access to $V_m$, however, and so we might also ask how well we can estimate cortical UP/DOWN states from LFP alone. A simple thresholding on the vertical axis of Fig. 2(f) would not solve this problem. However, taking into account the dynamics of the LFP trajectory, it is apparent that some progress might in fact be made. Figure 2(g) shows the trajectory of low frequency (< 2 Hz) component of the LFP, indicate nontrivial dynamics including hysteresis. Plotting the phase, $\varphi_X(t)$, in this band explicitly (Fig. 2(h)) suggests that LFP phase may, as suggested above, be a good way to look at cortical state trajectory, as substantial transitions in $V_m$ seem to occur only in a narrow range of phases. Other frequency bands may also provide similar information. Especially, as membrane potential oscillations corresponding to switching between UP and DOWN states are accompanied by an increased power in the slow (< 1 Hz) and delta (1–4 Hz) bands of the EEG (Destexhe et al. 1999, Li et al. 2009). This suggests that the frequencies < 4 Hz may provide much of the information about cortical UP and DOWN states.

In order to further explore the relationship between the phase of the LFP in different frequencies and the cortical trajectory, we filtered the LFP into four frequency bands (< 2, 2–4, 4–7 and 7–9 Hz), calculating phase, $\varphi_X(t)$, in each band as described in Section 2.3. Figure 3(a) shows the components of an example LFP trace, broken into components from each frequency band; the individual traces are colored according to the $V_m$ -defined state at that time instant. Figure 3(b) shows for each band the corresponding histogram of LFP phases, for both UP and DOWN states. We found that during an UP state (red distributions), the LFP phase distribution in the < 2 Hz and 2–4 Hz bands showed peaks at 226°±7° and 204°±9° respectively (mean±s.e.m, across the 9 recordings listed in Suppl. Table 1). The LFP phase distributions during DOWN states (blue distributions) in contrast peaked at 47° ±10° and 25°±9°, about 180° away from the peaks of the UP state distributions. In addition the standard deviation of the distributions increased at higher frequencies. The phase of the LFP in the frequency band of 4–7 Hz band showed a weak relationship to cortical UP/DOWN states, peaking at 203°±6° for the cortical UP state and 23°±9° for the cortical DOWN state. The 7–9 Hz band did not show a relationship to either of the cortical UP/DOWN states.

The differential likelihood of states, $L_X(\varphi_X)$, calculated in three frequency bands, < 2 Hz, 2–4 Hz and 4–7 Hz, is shown in Fig. 4(a). $L_X$ ranges between −1 and 1, and for values of $L_X$ close to 1, the network is likely to be in an cortical UP state, and close to −1 it is likely to be in a cortical DOWN state. $L_X$ in each frequency band showed a near sinusoidal relationship with LFP phase, $\varphi_X$ When fitted by a cosine (by minimizing *MSE* in Eq. (4)), $L_X(\varphi_X)$ peaked at ($\theta_x$ = mean±s.d., across the 9 recordings listed in Suppl. Table 1) 236° ± 18°, 215°±17° and 211°±20° for frequency bands < 2, 2–4 and 4–7 Hz respectively. The low standard deviations of the fitted $\theta_x$ indicate that the phase relationship between LFP phase and cortical UP/DOWN states is consistent across recordings.

To examine whether the relationship between $L_X$ and $\varphi_X$ is affected by the presence of a stimulus, in Fig. 4(b) we plotted the mean $L_X(\varphi_X)$ across recordings with no stimulus present, compared to the mean $L_X(t)$ under either ‘puretone’ or ‘AM-noise’ stimulation. The relationship between the phase of LFP and differential likelihood of states during sensory evoked activity was strikingly similar to their relationship during spontaneous activity.

As the whole-cell and LFP recordings were recorded from different sites, it is possible that the relationship between $L_X$ and $\varphi_X$ is critical to their relative position. Hence, in Fig. 4(c) we plotted $L_X(\varphi_X)$ calculated from the different LFP recording sites on the silicon micro electrode array (each from a different tetrode). The relationship between $L_X$ and $\varphi_X$ is similar across the different recording sites, which suggests that $L_X(\varphi_X)$ is not critical to the distance between the LFP and whole-cell electrode sites, up to a distance of 300 μm (half-width of the silicon micro electrode array).

## 4 Detection of cortical UP and DOWN states from extracellular signals

Having verified that extracellular signals contain information about cortical UP/DOWN states, we set out to develop a method to detect the network state based on this activity. Here we compare several approaches to this problem. Firstly, we introduce an algorithm based on the phase of low frequency components of the LFP. We compare this with an approach based on MUA, as utilized by previous authors (Hasenstaub et al. 2007, Luczak et al. 2007). Finally, we introduce an algorithm combining MUA and LFP phase information.

As described in Sec. 3.2, The $S_{LFP}(t)$ has a high correlation with the $V_m$ (0.66±0.03), which can be observed in the example shown in Fig. 5(a). Also, the distribution of $S_{LFP}(t)$ is bi-modal, as is the distribution of membrane potential (top of Fig. 5(a) and right of Fig. 5(c)). A second example is shown in Suppl. Fig. S1.

As the multi-unit activity itself is correlated with the membrane potential as described in Section 3, MUA was directly used as the evidence variable, $S_{MUA:yyy}$, over which a decision regarding the instantaneous state can be made (Eq. (9)). An example of $S_{MUA:all}$ is shown in Fig. 5(b). In contrast to the distribution of $S_{LFP}$, the distribution of $S_{MUA:all}$ shows no clear bimodality (see top of Fig. 5(b)), which makes it difficult to select thresholds over the decision variable, $S_{MUA:all}$, to detect state.

The linear combination of $S_{LFP}$ and $S_{MUA:all}$ results in a decision variable that is more tightly correlated with $V_m$ (correlation coefficient of 0.75±0.02) than $S_{LFP}$ (0.66± 0.03) and $S_{MUA:all}$ (0.69±0.03) (mean±s.e.m, across the 9 recordings listed in Suppl. Table 1). It indicates that $S_{LFP}$ and $S_{MUA:all}$ indeed have some independent information regarding the cortical UP/DOWN states and raises the possibility that the evidence variable $S_{Comb}$ may perform well at discriminating between the UP and DOWN states.

To evaluate the performance of each of these decision variables ($S_{LFP}$, $S_{MUA}$ under several different MUA definitions, and $S_{Comb}$) we used ROC analysis (Green and Swets 1966). ROC analysis evaluates how well a binary classification can be made. The ROC curve characterizes discriminability across all values of the thresholding criterion applied to the decision or evidence variable, thus allowing performance to be examined for all policies of the fraction of correct detections required, or false positives that can be tolerated. As ROC analysis is for binary classification, points when the membrane potential fell between the two thresholds (indeterminate points) were not considered in the analysis. The ideal classification algorithm should provide a high true positive rate and low false positive rate, with its ROC curve going as close as possible to the left top corner of the plot. DOWN state classification is made similarly; for visualization purposes, this is shown on Fig. 5(d) mirrored about the diagonal. The area under the ROC curve gives an estimate of how discriminable the two states are, on the basis of the particular evidence variable used, regardless of the ultimate user choice of policy (correct detections required and false positives tolerated). ROC areas close to 0.5 (curve along the diagonal) indicate chance discriminability and values close to 1, near perfect discriminability.

We first used the ROC analysis to evaluate the contribution to UP/DOWN state discriminability of the different frequency bands. The areas under the ROC curves for a number of different frequency band selections are shown in Fig. 5(e). When the phase from each frequency band was used independently, the < 2 Hz band outperformed the 2–4 Hz and 4–7 Hz bands, with the later performing only slightly above chance levels (area ~0.6). There was a small increase (1.25%) in performance when combining the < 2 Hz and 2–4 Hz bands, while no further increase could be seen by adding the 4–7 Hz band. The UP and DOWN state detection perform at nearly equal levels for the different frequency ranges.

Having found that the evidence variable for $S_{LFP}$ performed best when considering < 4 Hz frequencies, we compared it against evidence variables calculated using other sources of information, $S_{MUA}$ under different MUA definitions and $S_{Comb}$. In the example shown in Fig. 5(d), $S_{LFP}$ performed better than any of the evidence variables for multi-unit activity, $S_{MUA:sin}$, $S_{MUA:tet}$ and $S_{MUA:all}$. The area under the respective ROC curves, shown in Fig. 5(f), makes this clearer as the ROC curve for $S_{LFP}$ has an area of 0.9± 0.02, on average across all recordings, while those of multi-unit activity, $S_{MUA:sin}$, $S_{MUA:tet}$ and $S_{MUA:all}$ reach 0.85± 0.02, 0.83±0.03 and 0.85±0.02 (mean±s.e.m, across the 9 recordings listed in Suppl. Table 1). $S_{Comb}$ performs better than any of the other classification algorithms studies, performing with an ROC area of 0.92±0.02. One interesting feature that the ROC analysis shows is that the multi-unit activity based evidence variables ($S_{MUA:sin}$, $S_{MUA:tet}$ and $S_{MUA:all}$) are better at detecting DOWN states compared to UP states. All the evidence variables tested perform quite well with area under the ROC curves well above chance levels, ranging from 0.82 to above 0.92.

The calculation of $S_{LFP}$, and hence the detection of cortical UP and DOWN states, is based on two parameters, $\theta'_{<2}$ and $\theta'_{2-4}$ (where the subscript refers to the frequency band). While we use Eq. (6) to estimate these parameters, are these values optimal to detect the cortical UP/DOWN states? To examine this, we calculated the performance (measured as the difference between 'true positive rate' and 'false positive rate') for different values of the parameters, $\theta'_{<2}$ and $\theta'_{2-4}$, between 0° to 360° (in steps of 20°). Figure 6(b) shows of the performance as a function of $\theta'_{<2}$ and $\theta'_{2-4}$ for an example recording and Fig. 6(a) shows the same, averaged across all recordings. The values of the parameters chosen from Eq. (6), shown in red, are within the area of high performance. The flat peaks (white regions in Fig. 6(a and b)) of performance, indicate that the analysis is not sensitive to the precise values of the parameters, $\theta'_{<2}$ and $\theta'_{2-4}$.

In the performance measurements described above, we have been assuming that the membrane potential of a single, randomly selected neuron provides a good measure of the "ground truth" cortical UP/DOWN state. In fact, this may not always be the case: it may be that in some instances, the cell does not behave the same way as the average activity of the network, or that different subnetworks are behaving differently. Another way to examine how well our approach performs is to simply examine the state transitions detected by the algorithm, and consider whether they are consistent and reasonable given the other variables recorded. Figure 7 shows an example of this qualitative analysis, for a dataset to which the LFP phase based state detection algorithm has been applied (i.e. using evidence variable $S_{LFP}$). The distinction between UP and DOWN state thresholds can be seen in Fig. 7(a and b), leading to criteria which separate the evidence variable $S_{LFP}$ into regions clearly identifiable with the modes of the bimodal distribution, and an unclassifiable region in between. To verify that the times of state transitions are systematically consistent between LFP and $V_m$ driven definitions, we compared the transition-triggered averages of the MUA (Fig. 7(c)) and LFP (Fig. 7(d)). The shape and temporal width of the transition triggered average MUA and LFP kernels were extremely similar whether membrane potential or LFP is used to derive transition times. The qualitative correspondence of the state transition

timing using the two information sources is shown in Fig. 7(e, f): the LFP-derived algorithm has wider regions during which the state can not be assigned (although potentially this could be tuned out, at the expense of an increased false-positive rate).

## 5 Discussion

We have found that the phase of LFP with respect to frequencies in the signal below 4 Hz provided the most information about the instantaneous state of the intracellularly recorded neuron. Based on these findings, we developed an algorithm for detecting the instantaneous cortical UP/DOWN state based on the phase of the recorded LFP. This method performs substantially better than detection based purely on multi-unit activity. However, combining evidence from the multi-unit activity with that from LFP phase further improves state detection performance.

Most studies exploring the effect of state on cortical processes rely on intracellular recordings to determine cortical state. Detecting state, a network level phenomenon, based on the membrane potential of a single, randomly selected neuron may be biased towards arbitrary fluctuations of that neuron. In fact, the precise timing of transitions in the membrane potentials of simultaneously recorded units does not always coincide (Petersen et al. 2003; Lampl et al. 1999). Network level measures of activity like LFP or multi-unit activity average the activity of populations of neurons, smoothing out any fluctuations of single neurons from the population average. We evaluated performance of different evidence variables by comparing them with the $V_m$-defined state as the “ground truth”. However, the state detected on the basis of evidence variables (like $S_{Comb}$) calculated from the measures of network activity might be a more reliable estimate of the cortical UP/DOWN state.

The evidence variable $S_{LFP}$ was calculated based on two parameters, $\theta'_{<2}$ (mean value=236°) and $\theta'_{2–4}$ (mean value= 215°). These parameters were in turn calculated from the corresponding relationships between $L_X$ and $\varphi_X$. This relationship remains consistent across different recordings (Fig. 4(a)), during the presence or absence of a stimulus (Fig. 4(b)), and do not depend on the distance between the recording sites of the patch and LFP recordings (up to 300 μm, Fig. 4(c)). The large flat region of peak performance in Fig. 6(a and b) shows that the method is robust to small errors in choosing the two parameters. While the parameters provided in this paper are validated for recordings of the rat auditory cortex, a confirmatory whole-cell recording will be required to experimentally confirm the parameters in other areas of the cortex.

In the present study we have introduced a method of detecting network state based on the evidence variable $S_{LFP}$ and evaluated its performance in comparison with evidence variables calculated from multi-unit activity, $S_{MUA}$. In our recordings, detection algorithms making use of $S_{LFP}$ on average performed better than those based on $S_{MUA}$. It is however difficult to predict which will perform better for a different recording configuration. In fact in two of our nine recordings (Cell 5, R7 and Cell 3, R4 of nine recordings, R1–9), $S_{MUA:all}$ had a higher area under the ROC curve than $S_{LFP}$. Also, other recordings configurations might sample the MUA differently as compared to our setup. For instance, in an example shown by Hasenstaub et al. (2007), the authors find a correlation of 0.84 between $V_m$ and MUA:sin, after calculating MUA:sin based on extracellular recordings with a glass pipette, whereas for our recordings, where MUA:sin was derived from a multi-electrode array channel, an average correlation of 0.6 (best case correlation 0.81) was obtained. Thus we cannot predict whether $S_{LFP}$ will perform better than $S_{MUA}$. However, in all our recordings $S_{Comb}$ consistently outperformed the other evidence variables and as it combines

information from both $S_{LFP}$ and $S_{MUA}$ it is more likely to perform better across all recording configurations.

When a neuron is in a DOWN state, it is very unlikely to spike, and the distribution of its firing rate will be narrow and close to 0. However, the absence of spiking does not imply that the neuron is in a DOWN state, as there will be instances in time when a neuron does not spike even in an UP state. This will give rise to a region of overlap in the distributions of firing rates during UP and DOWN states. As we increase the number of neurons over which we pool the activity, this region of overlap between these distributions reduces and the performance of the detection of UP and DOWN states improves. Figure 5(f) shows this with the improvement of performance of $S_{MUA:all}$ over $S_{MUA:tet}$. Therefore, the performance of detecting instantaneous UP/DOWN states depends on how large a population of neurons is sampled, which would vary according to recording configuration. As the LFP reflects the input synaptic potentials and spiking activity of surrounding neural tissue (Eccles 1951; Katzner et al. 2009), it captures more global information which does not depend on the recording configuration.

The phase of the LFP at low frequencies combined with spiking activity, phase-coding, has been shown to convey about 50% more information regarding stimuli than spiking alone (Montemurro et al. 2008; Kayser et al. 2009). Here we show how the phase of the LFP also reveals the cortical state at that instant in time. Hence, the additional information regarding the stimulus in phase-coding could be attributed to state transitions explaining away part of the trial-to-trial variability (Carandini. 2004; Kisley and Gerstein 1999; Anderson et al. 2000). As state transitions are synchronized across the cortex (Li et al. 2009), this may allow downstream neurons to effectively interpret stimulus dependent information present in spike-trains.

The response properties of neurons have been shown to change depending on the state of the network (Anderson et al. 2000; Crochet and Peterson 2006; Sachdev et al. 2004; Haider et al. 2007; Hasenstaub et al. 2007). Recent technological advances are improving our ability to record well isolated spike trains from a large population of simultaneously recorded neurons using multi-electrode array recordings (Harris et al. 2000; Quiroga et al. 2004; Blanche et al. 2005; Maynard et al. 1997). This activity is strongly dependent upon network state under many conditions of interest; to interpret it, it is desirable to at the same time have an indicator of UP/DOWN states. Transitions in UP/DOWN states have also been used as temporal markers to study the affect of sleep homeostasis on cortical firing (Vyazovskiy et al. 2009), or investigate processing related to memory replay (Ji & Wilson 2007).

Whole cell patch clamp membrane potential recordings provide one approach to detecting cortical UP and DOWN states (Margrie et al. 2002). However, these recordings have a relatively low hit rate, and can often not be held as long as multi-electrode array recordings. The ability to reliably detect network state based purely on LFP and MUA recordings is demonstrated here during both spontaneous and evoked activity. This will allow the neural processing in large populations of neurons to be related to the UP/DOWN state dynamics of the brain, during both pharmacologically induced and natural brain states.

## Supplementary Material

Refer to Web version on PubMed Central for supplementary material.

## Acknowledgments

This research was funded by the Gatsby Charitable Foundation (grant GAT2830 to SRS), NIH (grant MH073245 to KDH), an NSF International Fellowship (IRFP-NSF 0804305 to JAS), and a Marie Curie Outgoing International Fellowship (PC).

## References

Anderson J, Lampl I, Reichova I, Carandini M, Ferster D. Stimulus dependence of two-state fluctuations of membrane potential in cat visual cortex. Nature Neuroscience. 2000; 3:617–621.

Arieli A, Sterkin A, Grinvald A, Aertsen A. Dynamics of ongoing activity: Explanation of large variability in evoked cortical responses. Science. 1996; 273:1868–1871. [PubMed: 8791593]

Azouz R, Gray CM. Cellular mechanisms contributing to response variability of cortical neurons *in vivo*. Journal of Neuroscience. 1999; 19:2209–2223. [PubMed: 10066274]

Bartho P, Hirase H, Monconduit L, Zugaro M, Harris KD, Buzsaki G. Characterization of neocortical principal cells and interneurons by network interactions and extracellular features. Journal of Neurophysiology. 2004; 92:600–608. [PubMed: 15056678]

Blanche TJ, Spacek MA, Hetke JF, Swindale NV. *Polytrodes: high-density silicon* electrode arrays for large-scale multiunit recording. Journal of Neurophysiology. 2005; 93:2987–3000. [PubMed: 15548620]

Carandini M. Amplification of trial-to-trial response variability by neurons in visual cortex. PLoS Biology. 2004; 2(9):e264. [PubMed: 15328535]

Compte A, Sanchez-Vives MV, McCormick DA, Wang XJ. Cellular and network mechanisms of slow oscillatory activity (<1 Hz) and wave propagations in a cortical network model. Journal of Neurophysiology. 2003; 89:2707–2725. [PubMed: 12612051]

Contreras D, Steriade M. Cellular basis of EEG slow rhythms: a study of dynamic corticothalamic relationships. Journal of Neuroscience. 1995; 15:604–622. [PubMed: 7823167]

Cossart R, Aronov D, Yuste R. Attractor dynamics of network UP states in the neocortex. Nature. 2003; 423:283–288. [PubMed: 12748641]

Cowan RL, Wilson CJ. Spontaneous firing patterns and axonal projections of single corticostriatal neurons in the rat medial agranular cortex. Journal of Neurophysiology. 1994; 71:17–32. [PubMed: 8158226]

Creutzfeldt OD, Watanabe S, Lux HD. Relations between EEG phenomena and potentials of single cortical cells. I. Evoked responses after thalamic and epicortical stimuluation. Electroencephalography and clinical neurophysiology. 1966a; 20(1):1–18. [PubMed: 4161317]

Creutzfeldt OD, Watanabe S, Lux HD. Relations between EEG phenomena and potentials of single cortical cells. II. Spontaneous and convulsoid activity. Electroencephalography and clinical neurophysiology. 1966b; 20(1):19–37. [PubMed: 4161316]

Crochet C, Peterson CCH. Correlating whisker behavior with membrane potential in barrel cortex of awake mice. Nature Neuroscience. 2006; 9:608–610.

Curto C, Sakata S, Marguet S, Itskov V, Harris KD. A simple model of cortical dynamics explains variability and state-dependence of sensory responses in urethane-anesthetized auditory cortex. Journal of Neuroscience. 2009; 29(34):10600–10612. [PubMed: 19710313]

Destexhe A. Self-sustained asynchronous irregular states and Up-Down states in thalamic, cortical and thalamocortical networks of nonlinear integrate-and-fire neurons. Journal of Computational Neuroscience. 2009; 27(3):493–506. [PubMed: 19499317]

Destexhe A, Contreras D, Steriade M. Spatiotemporal analysis of local field potentials and unit discharges in cat cerebral cortex during natural wake and sleep states. Journal of Neuroscience. 1999; 19:4595–4608. [PubMed: 10341257]

Destexhe A, Hughes SW, Rudolph M, Crunelli V. Are corticothalamic ‘up’ states fragments of wakefulness? Trends in Neurosciences. 2007; 30(7):334–342. [PubMed: 17481741]

Eccles JC. Interpretation of action potentials evoked in the cerebral cortex. Electroencephalography and clinical neurophysiology. 1951; 3(4):449–464. [PubMed: 14887631]

Green, DM.; Swets, JA. Signal detection theory and psychophysics. New York: Wiley; 1966.

Haider B, Duque A, Hasenstaub AR, McCormick DA. Neocortical network activity *in vivo* is generated through a dynamic balance of excitation and inhibition. Journal of Neuroscience. 2006; 26:4535–4545. [PubMed: 16641233]

Haider B, Duque A, Hasenstaub AR, Yu Y, McCormick DA. Enhancement of visual responsiveness by spontaneous local network activity *in vivo*. Journal of Neurophysiology. 2007; 97:4186–4202. [PubMed: 17409168]

Harris KD, Henze DA, Csicsvari J, Hirase H, Buzsaki G. Accuracy of tetrode spike separation as determined by simultaneous intracellular and extracellular measurements. Journal of Neurophysiology. 2000; 84(1):401–414. [PubMed: 10899214]

Hasenstaub AR, Sachdev RN, McCormick DA. State changes rapidly modulate cortical neuronal responsiveness. Journal of Neuroscience. 2007; 27:9607–9622. [PubMed: 17804621]

Hoffman KL, Battaglia FP, Harris KD, Maclean JN, Marshall L, Mehta MR. The upshot of up states in the neocortex: from slow oscillations to memory formation. Journal of Neuroscience. 2007; 27(44):11838–11841. [PubMed: 17978020]

Holcman D, Tsodyks M. The emergence of Up and Down states in cortical networks. PLoS Computational Biology. 2006; 2(3):e23. [PubMed: 16557293]

Ji D, Wilson MA. Coordinated memory replay in the visual cortex and hippocampus during sleep. Nature Neuroscience. 2007; 10(1):100–107.

Kandel A, Buzsaki G. Cellular-synaptic generation of sleep spindles, spike-and-wave discharges, and evoked thalamocortical responses in the neocortex of the rat. Journal of Neuroscience. 1997; 17:6783–6797. [PubMed: 9254689]

Katzner S, Nauhaus I, Benucci A, Bonin V, Ringach D, Carandini M. Local origin of field potentials in visual cortex. Neuron. 2009; 61(1):35–41. [PubMed: 19146811]

Kayser C, Montemurro MA, Logothesis NK, Panzeri S. Spike-phase coding boosts and stabilizes information carried by spatial and temporal spike patterns. Neuron. 2009; 61(4):597–608. [PubMed: 19249279]

Kisley MA, Gerstein GL. Trail-to-trail variability and state-dependent modulation of auditory-evoked responses in cortex. Journal of Neuroscience. 1999; 19(23):10451–10460. [PubMed: 10575042]

Lampl I, Reichova I, Ferster D. Synchronous membrane potential fluctuations in neurons of the cat visual cortex. Neuron. 1999; 22(2):361–374. [PubMed: 10069341]

Li CT, Poo M, Yang D. Burst spiking of a single cortical neuron modifies global brain state. Science. 2009; 324:643–646. [PubMed: 19407203]

Luczak A, Bartho P, Marguet SL, Buzsaki G, Harris KD. Sequential structure of neocortical spontaneous activity *in vivo*. Proceedings of the National Academy of Sciences of the United States of America. 2007; 104:347–352. [PubMed: 17185420]

Luczak A, Bartho P, Harris KD. Spontaneous events outline the realm of possible sensory responses in neocortical populations. Neuron. 2009; 62(3):1–13. [PubMed: 19376059]

Margrie TW, Brecht M, Sakmann B. *In vivo*, low-resistance, whole-cell recordings from neurons in the anaesthetized and awake mammalian brain. Pflugers Archive European Journal of Physiology. 2002; 444(4):491–498. [PubMed: 12136268]

Maynard EM, Nordhausen CT, Normann RA. The Utah intracortical electrode array: a recording structure for potential brain-computer interfaces. Electroencephalography and Clinical Neurophysiology. 1997; 102(3):228–239. [PubMed: 9129578]

Montemurro MA, Rasch MJ, Murayama Y, Logothetis NK, Panzeri S. Phase-of-firing coding of natural visual stimuli in primary visual cortex. Current Biology. 2008; 18(5):375–380. [PubMed: 18328702]

Parga N, Abbott LF. Network model of spontaneous activity exhibiting synchronous transitions between up and down states. Front. Neurosci. 2007; 1(1):57–66. [PubMed: 18982119]

Paxinos, G.; Watson, C. The rat brain in stereotaxic coordinates—the new coronal set. 5th ed.. New York: Academic; 2004.

Petersen CC, Hahn TT, Mehta M, Grinvald A, Sakmann B. Interaction of sensory responses with spontaneous depolarization in layer 2/3 barrel cortex. Proceedings of the National Academy of Sciences of the United States of America. 2003; 100:13638–13643. [PubMed: 14595013]

Poulet JF, Petersen CC. Internal brain state regulates membrane potential synchrony in barrel cortex of behaving mice. Nature. 2008; 454:881–885. [PubMed: 18633351]

Quiroga RQ, Nadasdy Z, Ben-Shaul Y. Unsupervised spike detection and sorting with wavelets and superparamagnetic clustering. Neural Computation. 2004; 16(8):1661–1687. [PubMed: 15228749]

Reig R, Gallego R, Nowak LG, Sanchez-Vives MV. Impact of cortical network Activity on short-term synaptic depression. Cerebral Cortex. 2006; 16(5):688–695. [PubMed: 16107589]

Renart A, de la Rocha J, Hollender L, Parga N, Reyes A, Harris KD. The asynchronous state in cortical circuits. Science. 2010; 327(5965):587–590. [PubMed: 20110507]

Sachdev RN, Ebner FF, Wilson CJ. Effect of subthreshold up and down states on the whisker-evoked response in somatosensory cortex. Journal of Neurophysiology. 2004; 92:3511–3521. [PubMed: 15254074]

Sakata S, Harris KD. Laminar structure of spontaneous and sensory-evoked population activity in auditory cortex. Neuron. 2009; 64(3):404–418. [PubMed: 19914188]

Sanchez-Vives MV, McCormick DA. Cellular and network mechanisms of rhythmic recurrent activity in neocortex. Nature Neuroscience. 2000; 3:1027–1034.

Shu Y, Hasenstaub A, McCormick DA. Turning on and off recurrent balanced cortical activity. Nature. 2003; 423:288–293. [PubMed: 12748642]

Steriade M, Nunez A, Amzica F. A novel slow (< 1 Hz) oscillation of neocortical neurons *in vivo*: depolarizing and hyperpolarizing components. Journal of Neuroscience. 1993; 13(8):3252–3265. [PubMed: 8340806]

Steriade M, Timofeev I, Grenier F. Natural waking and sleep states: a view from inside neocortical neurons. Journal of Neurophysiology. 2001; 85:1969–1985. [PubMed: 11353014]

Timofeev I, Grenier F, Steriade M. Disfacilitation and active inhibition in the neocortex during the natural sleep-wake cycle: an intracellular study. Proceedings of the National Academy Sciences of the United States of America. 2001; 98(4):1924–1929.

Vyazovskiy VV, Olcese U, Lazimy YM, Faraguna U, Esser SK, Williams JC, et al. Cortical firing and sleep homeostasis. Neuron. 2009; 63(6):865–878. [PubMed: 19778514]

Wilson CJ, Groves PM. Spontaneous firing patterns of identified spiny neurons in the rat neostriatum. Brain Research. 1981; 220(1):67–80. [PubMed: 6168334]

Wilson CJ, Kawaguchi Y. The origins of two-state spontaneous membrane potential fluctuations of neostriatal spiny neurons. Journal of Neuroscience. 1996; 16:2397–2410. [PubMed: 8601819]

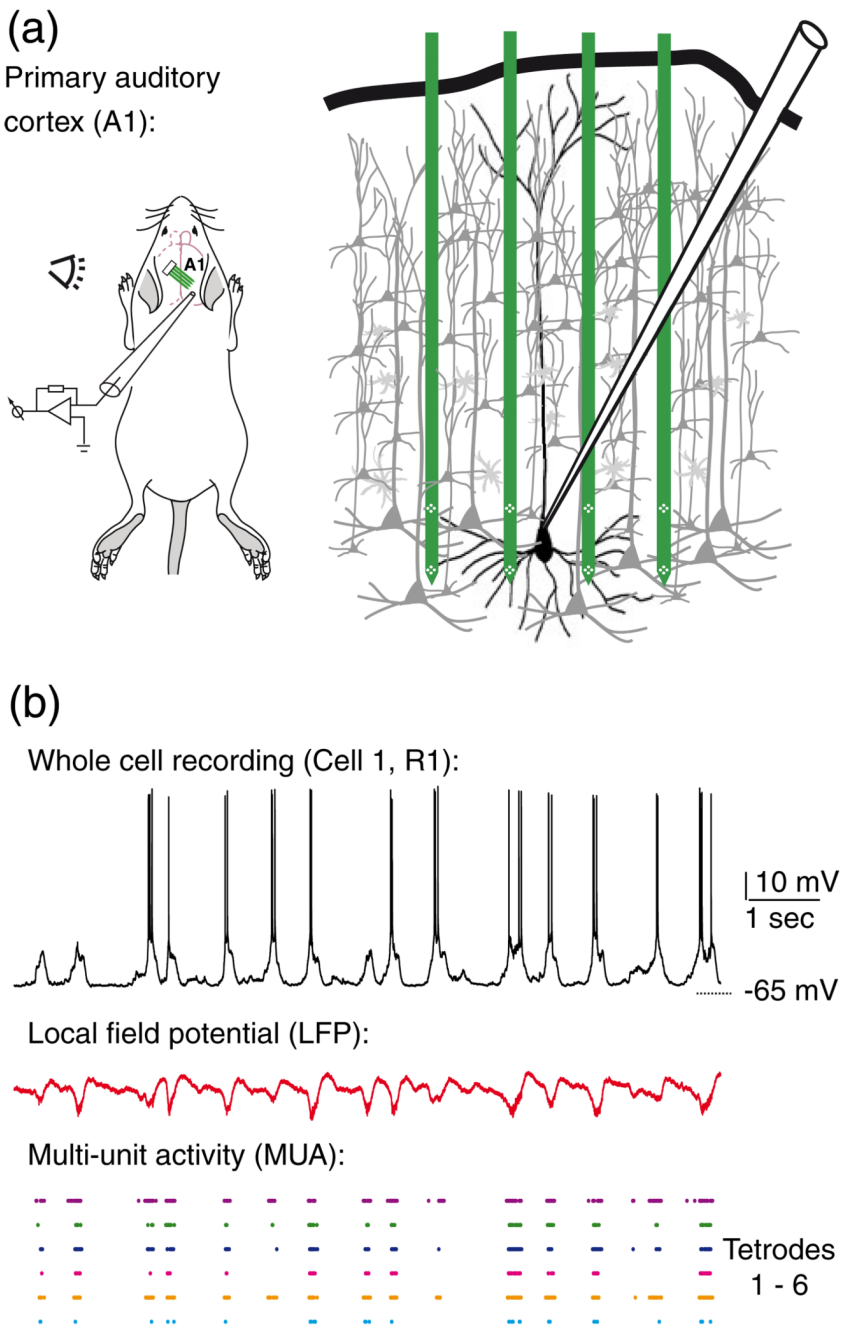


**Fig. 1.**

The 'patch-probe' recording configuration. **a**) An illustration of the recording setup where simultaneous whole-cell and MEA recordings were made from the rat auditory cortex. Four shank multi-electrode arrays were used, each shank (*green*) consisting of two tetrodes (*white diamonds*) totaling 32 recording sites. **b**) Examples (from Cell 1, R1) of simultaneously recorded whole cell (*top*), local field potential (*middle*) and sorted multi-unit activity (*bottom*) recordings

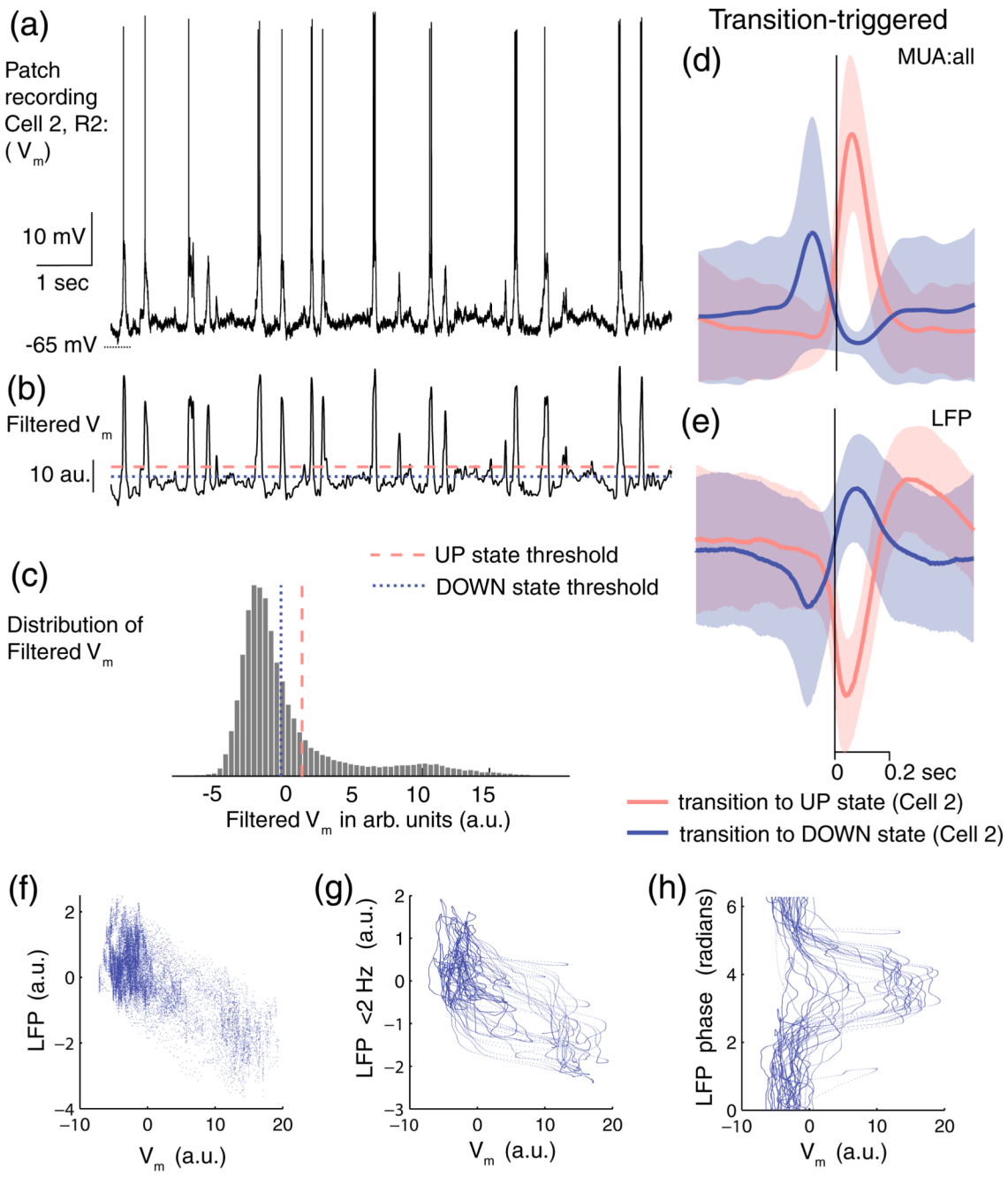


**Fig. 2.**

Intracellular and extracellular activity during network UP and DOWN states. Examples (from Cell 2, R2) of membrane potential ($V_m$) traces (**a**) before and (**b**) after filtering. (**c**) Histogram of the bimodal distribution of the filtered $V_m$. For this example, the dashed and dotted lines in (**b**) and (**c**) show the UP and DOWN discrimination thresholds used for state detection. (**d**) The transition-triggered average (*solid line*) and standard deviation (*shaded region*) of the MUA:all during transitions to UP states, red, and DOWN states, blue, in this example. (**e**) The transition-triggered average and standard deviation of LFP during transitions of UP (*red*) and DOWN (*blue*) states. Time is relative to state transitions detected using $V_m$ (*solid vertical line*). (**f**) LFP –$V_m$ relationship for a typical 20 sec. period of data.

(**g**) State dynamics in the low frequency LFP (< 2 Hz)— $V_m$ phase plane. (**h**) Phase dynamics over the same period

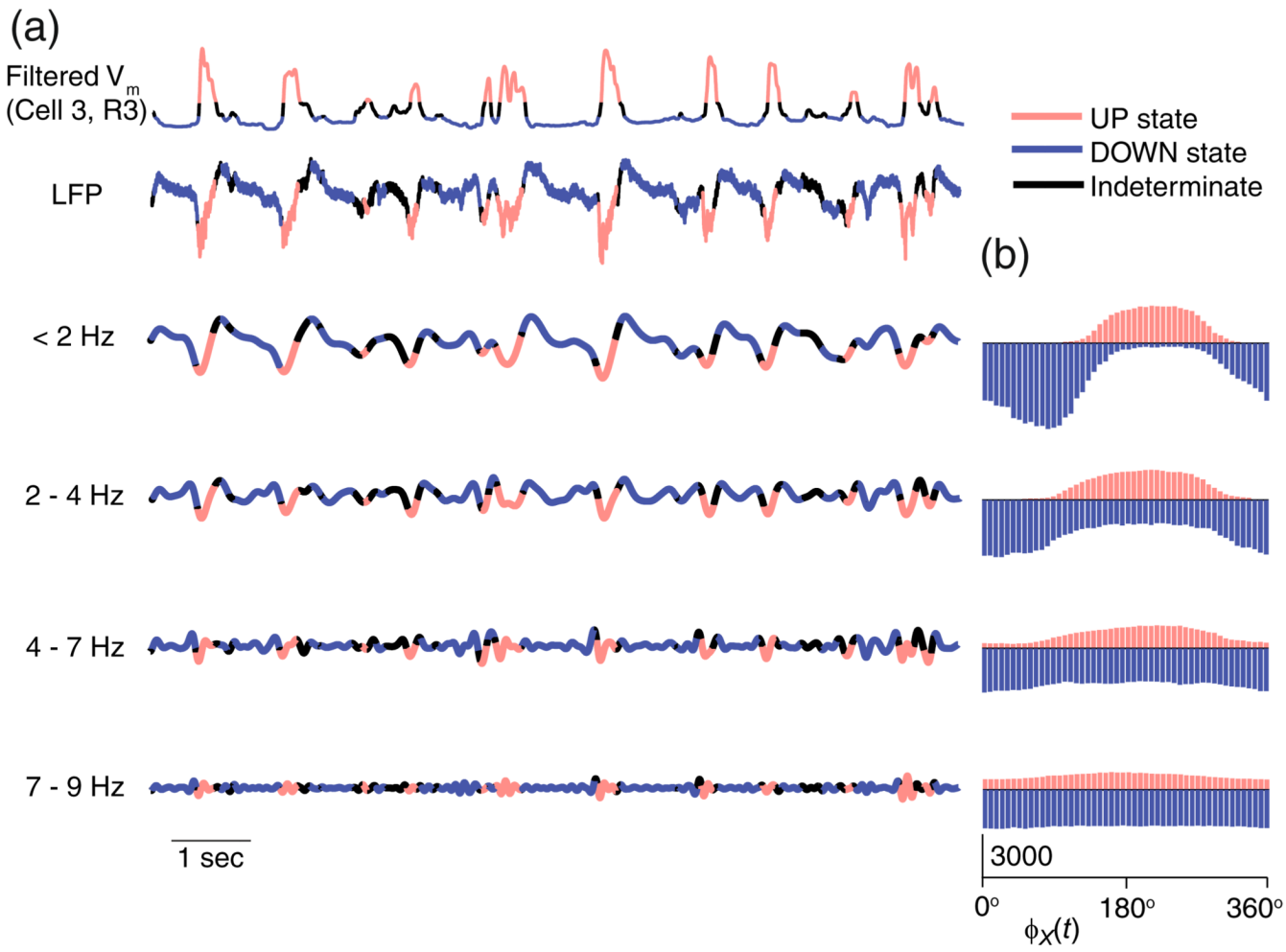


**Fig. 3.**

Network UP and DOWN states revealed in the phase of low frequency bands of the LFP. (**a**) Example (from Cell 3, R3) filtered $V_m$ and LFP traces with the periods of time spent in UP and DOWN states, as determined from filtered $V_{m,}$ indicated in red and blue, respectively. The LFP is shown split into four frequency bands < 2, 2–4, 4–7 and 7–9 Hz. The black regions are segments of time where the state was indeterminate since the filtered $V_m$ was between the two threshold values. (**b**) Histograms showing how often a particular LFP phase occurs during an UP (*red*) and DOWN (*blue*) state in the different frequency bands

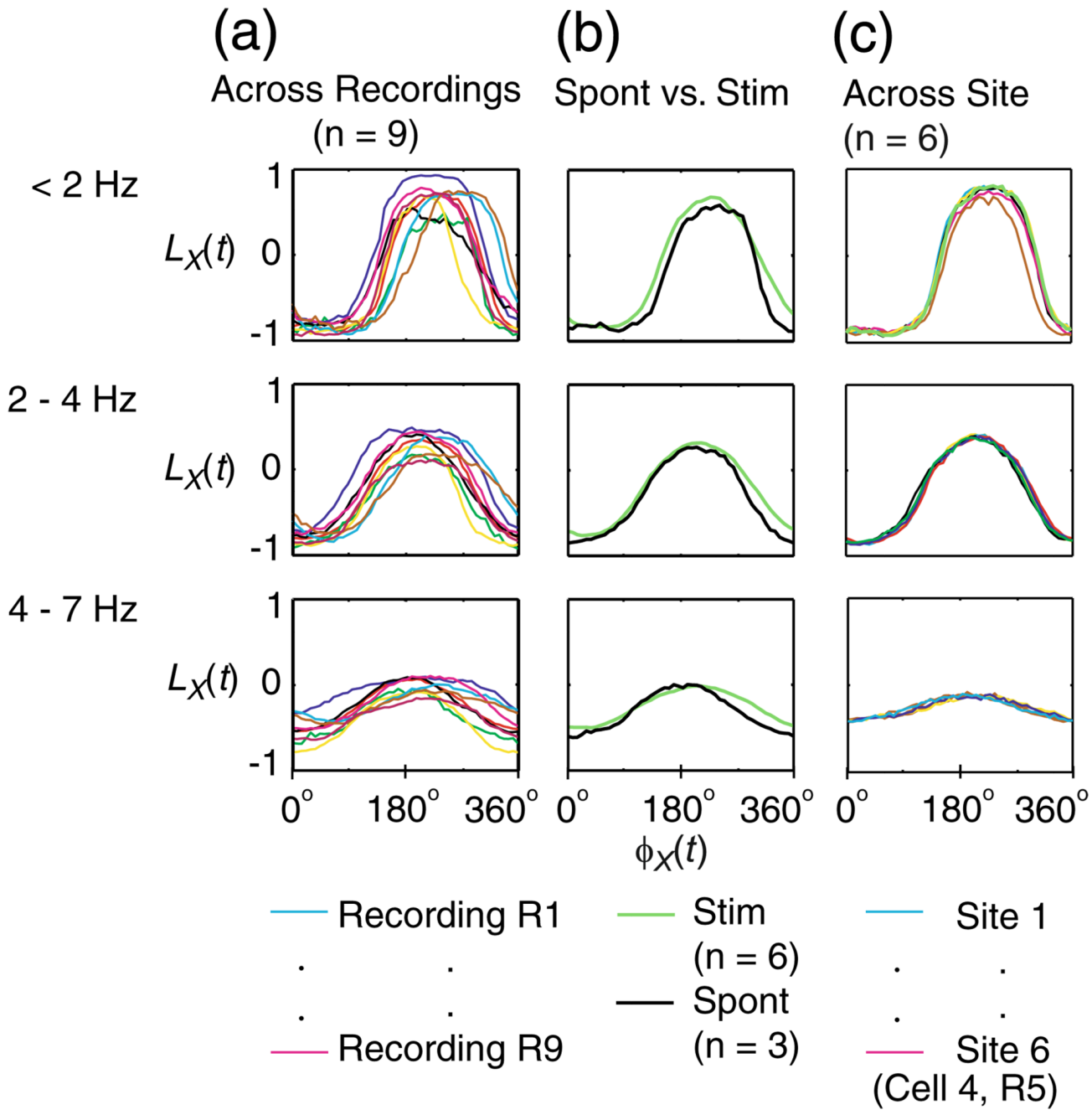


**Fig. 4.**

Differential likelihood of network state, $L_X(t)$, as a function of the phase of LFP in three frequency bands, < 2, 2–4 and 4–7 Hz. (**a**) The relationship of $L_X(t)$ to phase of LFP across the different recordings, represented in different colours and (**b**) in the presence (*green*) and absence (*black*) of an auditory stimulus

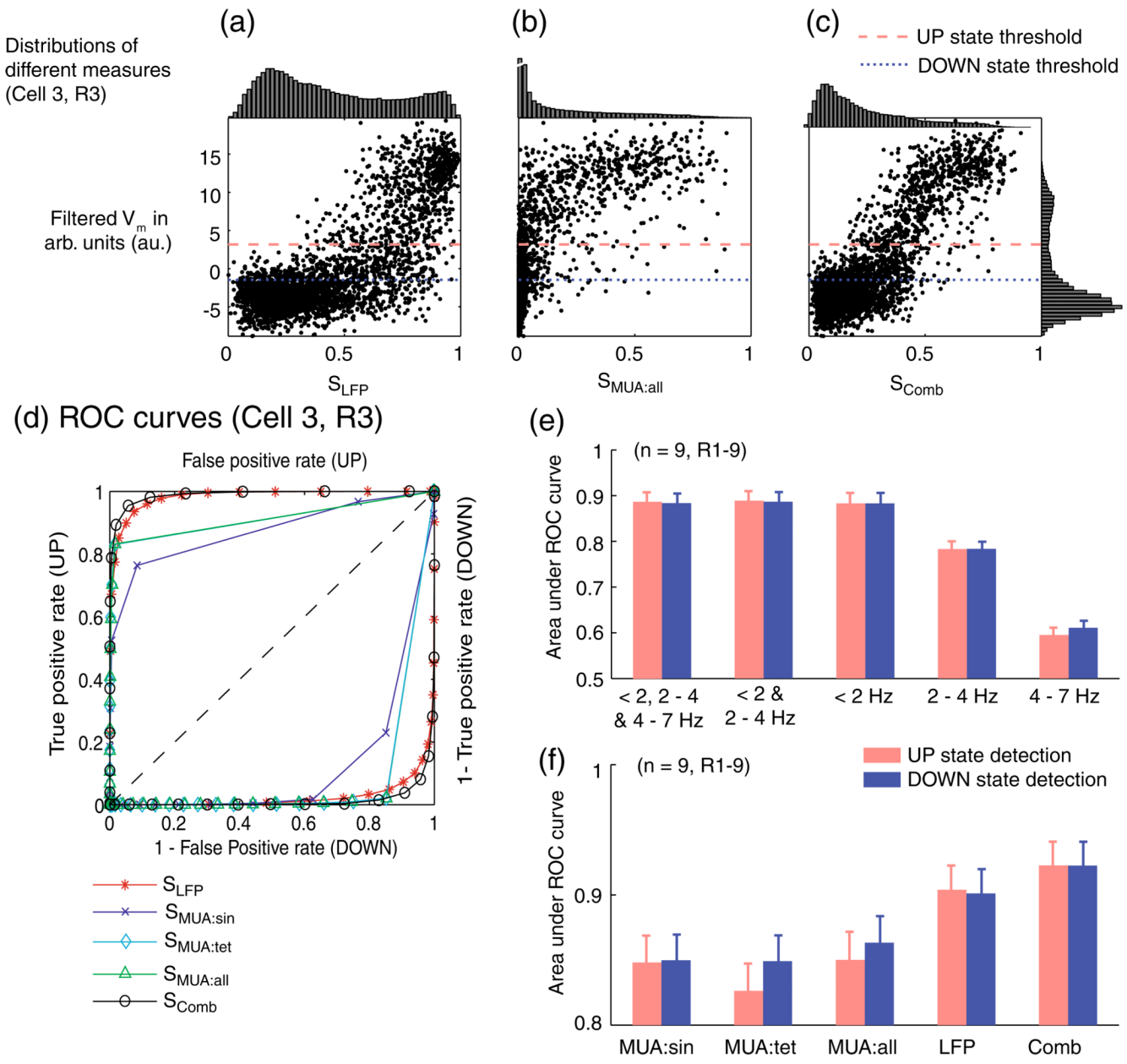


**Fig. 5.**

Comparison of the performance of evidence variables at network state detection. (**a–c**) Scatter plots of the filtered membrane potential (calculated on Cell 3, R3) versus evidence variables calculated from different measures of extracellular activity: (**a**) $S_{LFP}$, based on LFP; (**b**) $S_{MUA:all}$; (**c**) $S_{Comb}$, the linear summation of $S_{LFP}$and $S_{MUA:all}$. The distributions of the individual evidence variables (*top plots*) and the filtered $V_m$ (plot on the right of c) are shown. The dashed and dotted lines show the UP and DOWN discrimination thresholds. (**d**) ROC curves (from Cell 3, R3) for the detection of states using metrics $S_{LFP}$, $S_{MUA:sin}$, $S_{MUA:tet}$, $S_{MUA:all}$ and $S_{Comb}$. The top left half shows the ROC curves for the detection of UP states, while the bottom right half shows the ROC curves for the detection of DOWN states (Note that these curves are not symmetric). (**e**) The area under the ROC curve of the

metric S when using different frequency bands to calculate $S_{LFP}$ as well as for (**f**) the different metrics shown in d. Error bars in e and f are the s.e.m. calculated over R1–9

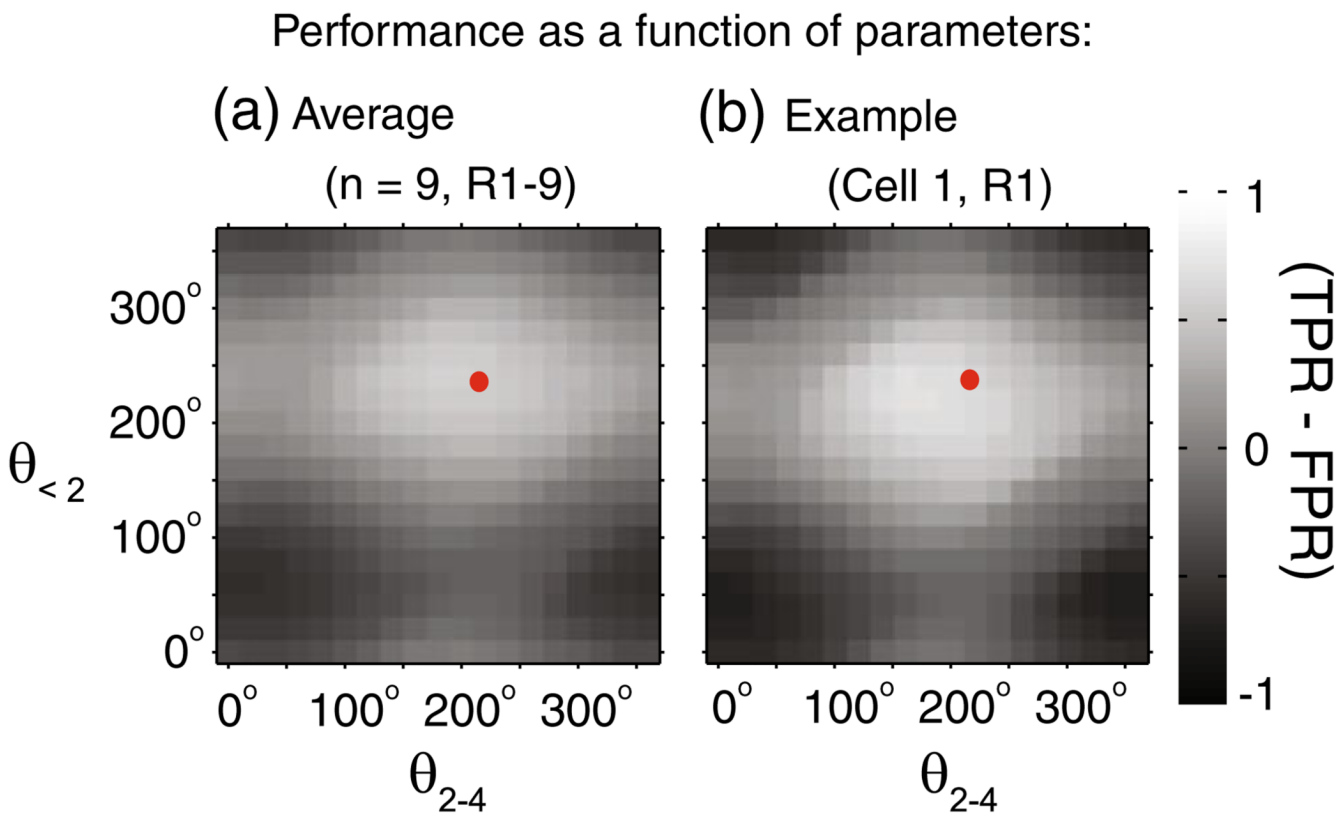


**Fig. 6.**

Performance of network UP and DOWN state detection as a function of chosen parameters. The performance of the detection of network UP and DOWN states based on $S_{LFP}$ is plotted as a function of the choice of parameters $\theta'_{<2}$ and $\theta'_{2-4}$ (TPR: True positive rate, FPR: False positive rate). (**a**) The average performance across all the $n$=9 recordings and (**b**) an example recording (from Cell 1, R1), as functions of $\theta'_{<2}$ and $\theta'_{2-4}$

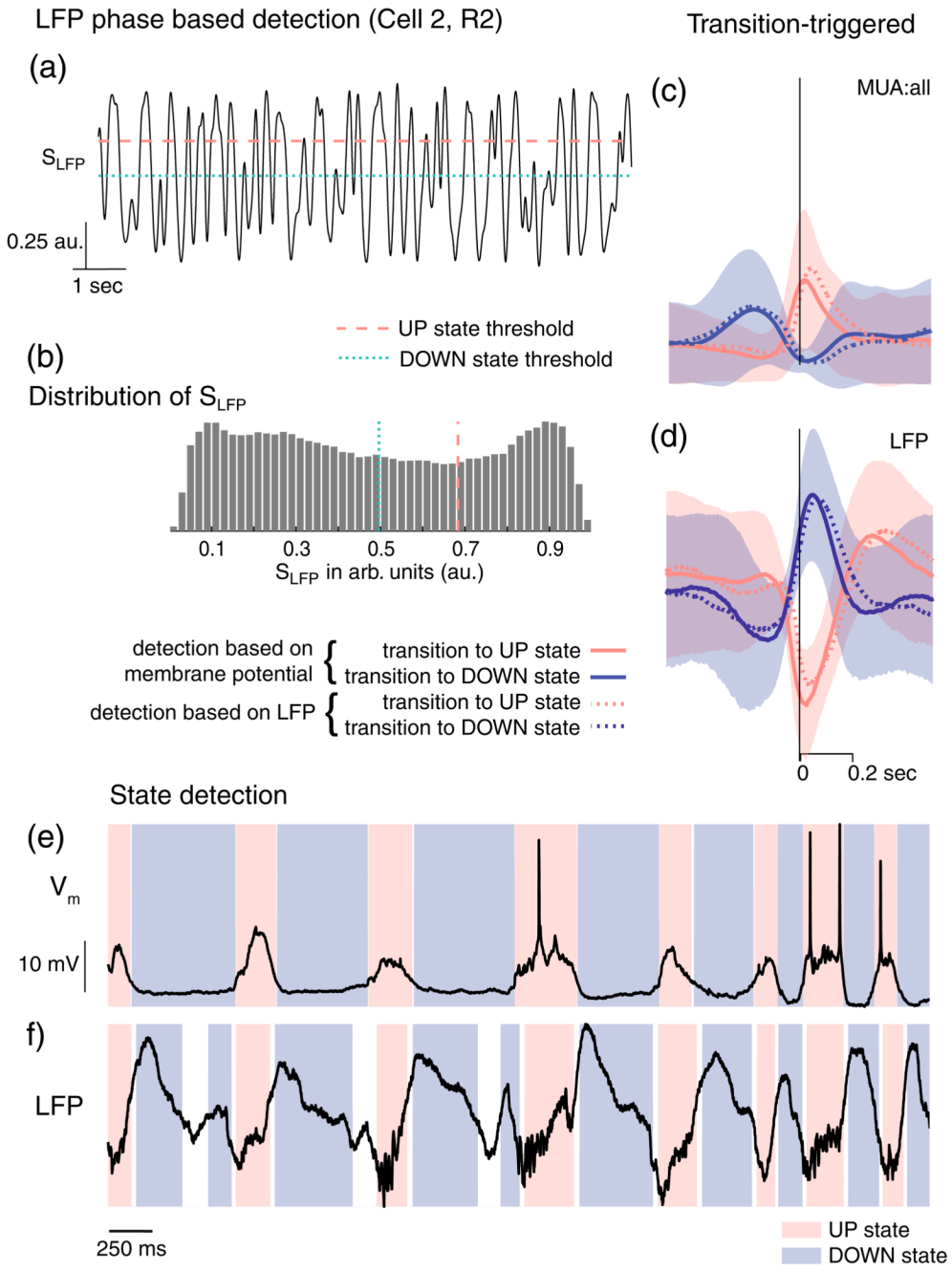


**Fig. 7.**

Qualitative comparison of state transitions detected from $V_m$ and the evidence variable $S_{LFP}$. (**a**) An example trace (from Cell 2, R2) showing how the evidence variable *S* varies in time. (**b**) The bi-modal distribution of $S_{LFP}$. The dashed and dotted lines in a and b show the UP and DOWN thresholds for detection used in this example. (**c**) The average (solid line) and standard deviation (shaded region) of the transition-triggered MUA:all during transitions to UP (red) or DOWN (blue) states. (**d**) The average and standard deviation of LFP during transitions of UP (red) or DOWN (blue) states. Time, in this case, is relative to state transitions as detected based on the LFP (vertical line). The dotted lines show the transition-triggered average LFP and MUA at state transitions detected based on the membrane

potential (shown in Fig. 2B). (**e**) The membrane potential, $V_m$; red-shaded regions correspond to $V_m$-detected UP states and blue-shaded regions correspond to $V_m$-detected DOWN states. (**f**) The corresponding LFP; here, the shaded regions correspond to the states detected using the algorithm based on $S_{LFP}$. Indeterminate regions in e and f are shown in white. e and f illustrate the close correspondence of the classification from $V_m$ and the evidence variable $S_{LFP}$